Cosmic Ray $e^+/(e^- + e^+)$, $\bar{p}/p$ Ratios Explained by an Injection Model Based on Gamma-ray Observations

T. Kamae[1,2], S.-H. Lee[1,3], L. Baldini[4], F. Giordano[5,6], M.-H. Grondin[7], L. Latronico[4], M. Lemoine-Goumard[7], C. Sgrò[4], T. Tanaka[1], Y. Uchiyama[1]

ABSTRACT

We present a model of cosmic ray (CR) injection into the Galactic space based on recent γ-ray observations of supernova remnants (SNRs) and pulsar wind nebulae (PWNe) by the *Fermi* Large Area Telescope (*Fermi*) and atmospheric Cherenkov telescopes (ACTs). Steady-state (SS) injection of nuclear particles and electrons (e^-) from the Galactic ensemble of SNRs, and electrons and positrons (e^+) from the Galactic ensemble of PWNe are assumed, with their spectra deduced from γ-ray observations and recent evolution models. The ensembles of SNRs and PWNe are assumed to share the same spatial distributions and the secondary CR production in dense molecular clouds interacting with SNRs is incorporated in the model. Propagation of CRs to Earth is calculated using GALPROP with 2 source distributions and 2 Galaxy halo sizes. We show that this observation-based model reproduces the positron fraction $e^+/(e^- + e^+)$ and antiproton-to-proton ratio ($\bar{p}/p$) reported by *PAMELA* reasonably well without calling for new sources. Significant discrepancy is found, however, between our model and the $e^- + e^+$ spectrum measured by *Fermi* below $\sim$ 20 GeV. Important quantities for Galactic CRs, including their energy injection, average lifetime, and mean gas density along their typical propagation path are also presented.

Subject headings: ISM: cosmic rays, ISM: supernova remnants, ISM: clouds, γ-rays: observations

[1]Kavli Institute for Particle Astrophysics and Cosmology and SLAC National Accelerator Laboratory, Stanford University, Stanford, CA 94305, USA

[2]email: kamae@slac.stanford.edu

[3]email: shia520@stanford.edu

[4]Istituto Nazionale di Fisica Nucleare, Sezione di Pisa, I-56127 Pisa, Italy

[5]Dipartimento di Fisica "M. Merlin" dell'Università e del Politecnico di Bari, I-70126 Bari, Italy

[6]Istituto Nazionale di Fisica Nucleare, Sezione di Bari, 70126 Bari, Italy

[7]Université Bordeaux 1, CNRS/IN2p3, Centre d'Études Nucléaires de Bordeaux Gradignan, 33175 Gradignan, France

Work supported in part by US Department of Energy contract DE-AC02-76SF00515.

SLAC National Accelerator Laboratory, Menlo Park, CA 94025

1. Introduction

Recent observation of the positron fraction, $e^+/(e^- + e^+)$, by *PAMELA* (Adriani et al. 2009a) shows an excess (referred to as the e^+ excess, or the excess in the positron fraction) relative to the prediction of a cosmic-ray (CR) propagation model (Moskalenko & Strong 1998) in the energy range between 10 and 100 GeV. The model referenced in most analyses of the e^+ excess is GALPROP version 98a[1] which assumes e^+ to be produced along the propagation path by the Galactic CR protons [2] having a power-law spectrum with a locally observed index of 2.75. A constraint applied to these analyses is that the spectrum predicted for $e^- + e^+$ or leptons[3] agrees with that measured by the *Fermi* Large Area Telescope (*Fermi*) (Abdo et al. 2009a, 2010j). Various additional sources of e^+ have been proposed to account for the e^+ excess, including pulsars (PSRs) and pulsar wind nebulae (PWNe) (e.g, Yüksel et al. 2009; Profumo 2008; Malyshev et al. 2009; Gelfand et al. 2009; Grasso et al. 2009; Kawanaka et al. 2010, and references therein); supernova remnants (SNRs) (e.g., Blasi 2009; Fujita et al. 2009; Ahlers et al. 2009, and references therein); propagation effects (e.g., Katz et al. 2010; Stawarz et al. 2010, and references therein); and dark matter (DM) annihilation or decay (e.g., Boezio et al. 2009; Grasso et al. 2009; Meade et al. 2010, and references therein). In some references, the e^+ excess is discussed together with a bump in the CR lepton spectrum claimed by *ATIC* (Chang et al. 2008). This bump has not been observed by Abdo et al. (2009a, 2010j) in the latest *Fermi* measurements. Hence we will not consider the *ATIC* bump in this paper.

Measurements of the antiproton-to-proton ratio ($\bar{p}/p$) have recently been extended to ~ 100 GeV by *PAMELA* (Adriani et al. 2009b). The reference model used in the analysis of the ratio is GALPROP98b which predicts $\bar{p}$ to be produced[4] in the same inter-stellar matter (ISM) by the same Galactic CRs as for e^+ (e.g., Moskalenko et al. 2002; Strong et al. 2004, and references therein). Some early measurements of the ratio at lower energies at ~ 10 GeV gave higher values than the GALPROP98b prediction, and possible contribution from the DM annihilation have been discussed by Bergström et al. (1999) and in references given in Moskalenko et al. (2002). The new *PAMELA* measurement agrees well with a recent GALPROP version labeled as DC in Moskalenko et al.

[1] We refer to specific versions of GALPROP by the year of publication if not labeled in the literature. A detailed description of different versions of GALPROP can be found at http://galprop.stanford.edu. Various results obtained with GALPROP are reviewed in Strong et al. (2007).

[2] Contribution of alpha particles and heavy ions to pion production is included in "protons" by scaling the cross-section by an effective 'nuclear enhancement factor' of 1.68 (Gaisser & Schaefer 1992). The known gamma-ray producing particle processes which do not go through neutral pions (e.g., $\eta^0 \rightarrow \gamma\gamma$ and direct photon production processes) are also included but contribute less than 1 % in the present energy range.

[3] We refer to e^- and e^+ collectively as "leptons" later in this paper. We note "leptons" include nominally muons, tau particles and neutrinos.

[4] We note that anti-neutrons are predicted to be produced about equally to or substantially more than $\bar{p}$ in the high energy *pp* interaction dependent upon the iso-spin nature of diquark pairs produced when the QCD color string breaks (Anticic et al. 2010). They decay to $\bar{p}$ with the lifetime of n. In GALPROP, the $\bar{p}$ inclusive cross section by Tan & Ng (1982) has been doubled to include them.

(2002). Hence we will not consider possible contribution to CR $\bar{p}$ from the DM annihilation in this paper.

In SNRs, γ, e^-, e^+, and $\bar{p}$ are produced in the pp interactions as secondary particles which can, in principle, account for the *PAMELA* e^+ excess. However, the yields of π^+, π^- and π^0 are predicted to be approximately equal for proton kinetic energies greater than ~ 10 GeV, hence the spectrum of e^+, a daughter of π^+ decay, is tightly constrained by the observed γ-ray spectrum of π^0 origin. We survey below SNR-based scenarios proposed to account for the e^+ excess. In the work by Blasi (2009), e^+ are assumed to be re-accelerated to enhance the positron fraction. The lepton spectrum will then become harder as energy increases until radiative cooling takes over in the multi TeV energy band. All charged CRs including $\bar{p}$ will also show similar spectral hardening (Blasi & Serpico 2009). Fujita et al. (2009) have assumed that e^+ are produced in dense clouds by nuclear CRs accelerated when the Local Bubble exploded. The dense clouds existing at that time are assumed to have been destroyed by now. In this scenario, we expect to find anisotropy in the arrival direction of high energy charged CRs and in the pionic γ-ray emissivity at local molecular clouds; this will be tested in future *Fermi* observations. Ahlers et al. (2009) have calculated the e^+ spectrum at Earth based on proton spectra deduced from the presumed pionic γ-ray spectra of TeV SNRs. These SNRs, however, do not represent the Galactic ensemble of SNRs as seen in recent *Fermi* observations (Abdo et al. 2009d, 2010a,d,h,i). Katz et al. (2010) claims that the e^+ excess comes out naturally if the radiative loss time is comparable to the propagation time ($\sim 10^7$ yr) for e^+ of energy ~ 30 GeV. The authors have assumed a non-standard propagation yet to be confirmed. Stawarz et al. (2010) note that the rollover in the high energy lepton spectrum (Abdo et al. 2009a; Aharonian et al. 2008a, 2009) can be explained by the Klein-Nishina effect in the radiative loss. They then note that the observed e^+ excess can be reproduced only if CRs propagate through high density regions ($n > 80$ cm^{-3}) and secondary positrons pass through regions where star light density is extremely high (energy density > 300 eV cm^{-3}).

Another group of papers claim that one or a few PWNe within a few 100 pc of the solar system can account for the e^+ excess (e.g. Yüksel et al. 2009; Profumo 2008; Grasso et al. 2009; Malyshev et al. 2009, and references cited therein). The PWNe are assumed to have accumulated high energy leptons over a few $\times 10$ kyr and have released them impulsively at the right timing such that the highest-energy particles are now reaching Earth. We note that local PWNe and SNRs have been considered as possible sources of CR positrons prior to the *PAMELA* experiments (e.g., Aharonian et al. 1995; Atoyan et al. 1995; Kobayashi et al. 2004, and references therein). According to the recent theoretical studies (e.g., Gaensler & Slane 2006), energetic leptons can be injected impulsively into Galactic space only when some condition is met in a short epoch in their life, and the probability of such a rare impulsive injection taking place right now from one of very few nearby PWNe is low. On the observational side, *HESS* has found several PWNe whose ages exceed ~ 30 kyr as discussed by Aharonian et al. (2006b); Gallant (2007); Funk (2007) and in references given in Mattana et al. (2009). *Fermi* has found GeV emission from Vela-X (Abdo et al. 2010e). The leptons responsible for the GeV emission have energy of a few $\times 10$ GeV and reside in

the halo of the PWN adjacent to the region where TeV emission has been found (Abdo et al. 2010e; Aharonian et al. 2006a). These observations in the GeV-TeV band as well as recent theoretical studies (Gaensler & Slane 2006; Zhang et al. 2008; Tanaka & Takahara 2010; Bucciantini et al. 2010) suggest CR leptons are released slowly from PWNe allowing a larger ensemble of Galactic PWNe than those within a few 100 pc of Earth to contribute to the CR lepton spectrum.

Grasso et al. (2009); Malyshev et al. (2009) considered a distribution of pulsars and PWNe within a few kpc of the solar system to be responsible for the *PAMELA* e^+ excess. Grasso et al. (2009) have fitted the positron fraction well by assuming an e^- spectrum softer than that used in GALPROPv44_500180, the reference widely used in this kind of analyses (Strong et al. 2004). In this scenario, the e^+ flux at higher energies are dominated by unidentified nearby PWNe. Recently Delahaye et al. (2010) studied possible energy ranges that nearby PSRs, PWNe, and SNRs contributed to the CR electrons and positrons at Earth. Their contributions are predicted to give a flat positron fraction at energies greater than 10 GeV.

Ioka (2008) has associated the e^+ excess to an impulsive injection of e^+ by a presumed historic gamma-ray burst (GRB) that created the Local Bubble. Possible association of the Local Bubble with a GRB has been suggested earlier (e.g., Perrot & Grenier 2003; Lallement et al. 2003): Perrot & Grenier (2003) have predicted the CR e^- spectrum at Earth will be be harder at higher energies ($E > 100$ GeV) in such a scenario and emissivities of γ-rays at local molecular clouds will show directional dependence at the ~ 50 % level. Future *Fermi* observations of γ-ray emission from local clouds will detect such a large anisotropy if it exists.

Numerous publications have attempted to associate the e^+ excess with annihilation and/or decay of dark matter particles (e.g., Boezio et al. 2009; Grasso et al. 2009; Meade et al. 2010, and references therein), in which a number of interesting possibilities are proposed. In this work, however, we will not discuss any dark matter related scenarios.

All publications surveyed above attempt to reproduce the e^+ excess by interpreting a number of known local objects as CR sources using adjust-to-fit CR injection spectra and/or adopting non-standard CR propagation processes. Although we cannot rule out all such possibilities, it is important to study how recent γ-ray observations constrain the positron fraction and the $\bar{p}/p$ ratio within the conventional framework. Another important issue with these publications is that spectra of γ, p, e^-, e^+ and $\bar{p}$ are analyzed more-or-less independently. If these CRs come from SNRs and PWNe, or are produced in nuclear interactions with molecular clouds and ISM gas, there will be strong correlations among their spectra. In particular, the CR e^- spectrum should not be treated independently of the CR p, e^+ and $\bar{p}$ spectra. We treat these data in the coherent framework of GALPROP by assuming the Galactic CRs are in their steady states.

In this work, we put the prime focus on the Galactic CR ratios (e^+ fraction and $\bar{p}/p$ ratio) and use published γ-ray observation results as consistency checks for our calculations. All Galactic CRs are assumed to be injected by the ensemble of SNRs and PWNe, or to result from their interactions with the interstellar gas in the Galaxy, or from clouds interacting with SNRs. The CR injection

processes are assumed to be in steady-state (SS). The adopted injection spectrum of protons from SNRs is constrained by the available observations of CR proton flux at Earth, and is similar to those assumed in recent *Fermi*analyses of the diffuse Galactic γ-ray emission by (Abdo et al. 2009c,g, 2010l). The injection spectrum of e^+ and e^- from PWNe is deduced from currently available γ-ray observations of PWNe by *Fermi* and *HESS*, guided by recent theoretical spectral evolution models. The CR propagation process is calculated within the robust GALPROP framework. The calculated local CR fluxes are renormalized to those observed at Earth, which determines the CR injection luminosities. We purposely remain blind to the measured positron fraction as well as the measured $\bar{p}/p$ ratio until the calculated results are compared with the measurements.

The major assumptions made in our model are summarized below:

1. CRs are injected from the Galactic ensembles of SNRs (primary particles: p, e^-; secondary particles e^-, e^+, $\bar{p}$) and PWNe (primary particles: e^-, e^+).

2. The primary p and e^- injected from the Galactic ensemble of SNRs have a common SS spectral shape with a fixed e/p ratio, except near the maximum energy where the e^- injection spectrum is corrected for radiative energy loss.

3. The primary e^- and e^+ injected from the Galactic ensemble of PWNe have a common SS spectral shape and injection luminosity.

4. The primary p spectrum injected from SNRs is constrained by the observed CR proton spectrum at Earth.

5. The secondary CR spectra injected from SNRs interacting with molecular clouds are calculated assuming the p injection spectrum obtained in (4) at the interacting sites. We use the $pp \rightarrow e^+, e^-$ cross-sections modeled by Kamae et al. (2005, 2006) and the $pp \rightarrow \bar{p}$ cross-section from Tan & Ng (1982, 1983a,b).

6. The primary CR spectrum injected from PWNe is deduced from γ-ray observations by *Fermi* and ACTs, and PWN evolution models, e.g. by Tanaka & Takahara (2010) and Zhang et al. (2008).

7. SNRs and PWNe are distributed identically in the Galaxy according to the parametric model implemented in GALPROP. Two different sets of parameters are used to test the robustness of the calculated results.

8. The propagation, interaction and energy loss of CRs from the sources to Earth are calculated using GALPROP with two different halo sizes. Propagation parameters such as diffusion coefficient and re-acceleration have been adjusted in the input parameters of GALPROP to reproduce the observed CR proton and lepton spectra, and the observed B/C ratio at Earth.

This paper is divided into the following sections: We describe the 3 CR source classes assumed here in section 2. The 2 spatial distribution models of SNR/PWN in the Galaxy are described in

section 3. CR injection from SNRs and PWNe are discussed in sections 4 and 5, respectively. In section 6, the calculated positron fraction and the $\bar{p}/p$ ratio are compared with observations and discussion is given thereon. We also present quantitative calculations on energetics and lifetimes of Galactic CRs in the section. Finally, the paper is concluded in section 7 with future prospects.

2. Three CR Source Classes

The model is divided into three source classes, each representing a specific class of CR injection sources assumed in this study. We use GALPROP, whenever possible, to calculate CR injection and propagation effects in the Galactic space. In special cases, however, CR propagation has been calculated using a propagation program specifically developed to accommodate, for example, non-power-law injection spectra and source distribution without cylindrical symmetry with respect to the Galactic Center. This will be discussed in more detail in the coming sections.

The three classes of CR sources are:

'SNR-propagation': This class includes the primary CRs (p and e^-) injected from the Galactic ensemble of SNRs, the secondary CRs (e^-, e^+, $\bar{p}$) and diffuse γ-rays (π^0 decay, bremsstrahlung and IC) produced along the propagation path of the primaries.

'PWN-propagation': This includes the primary e^- and e^+ injected from the Galactic ensemble of PWNe, and the diffuse γ-rays produced along their propagation path via bremsstrahlung and inverse Compton scattering (IC). The injection spectral shape is deduced from the γ-ray observations by *Fermi*and ACTs (see Table 1).

'SNR-cloud interaction': We assume that a fraction of CRs accelerated at SNRs are interacting with dense local clouds as found by *Fermi* in middle-aged SNRs e.g., W49B, W44, W51C, IC 443, and W28 (see Table 2). These interaction sites contribute through hadronic interactions to the injection of secondary particles, including $e^{+/-}$, $\bar{p}$, and γ-rays. Propagation of $e^{+/-}$ and $\bar{p}$ from this source class has been calculated with a simple propagation code described in the Appendix.

We use the conventional 2-dimensional propagation mode in GALPROP, for which the Galaxy boundary possesses cylindrical symmetry; we adopt $R_{\rm max} = 20$ kpc and $Z_{\rm max} = 4$ kpc (i.e. halo height) for the 'default' model. In addition, we also construct two alternative models to check the robustness of our results to the assumptions made for the source distribution and the Galaxy halo size. The first alternative model adopts a different parameter set for the spatial distribution, and the second has the halo height enlarged to $Z_{\rm max} = 10$ kpc. We note that our results are checked to be insensitive to the change of $R_{\rm max}$ from 20 kpc to 30 kpc. Also, we try to estimate, in the context of this SS picture of the Galaxy, the significance of the injection of CR positrons from nearby sources (within a few hundred parsec from Earth) to the reproduction of the *PAMELA* positron fraction. Contribution by these 'local' sources will be discussed in section 6.

3. Spatial Distribution of SNRs and PWNe

We study two spatial distribution models of CR sources, parameterized in the form of:

$$P(R,Z) \propto \left(\frac{R}{R_\odot}\right)^{\alpha} \times \exp\left(-\beta\left(\frac{R-R_\odot}{R_\odot}\right)\right) \times \exp\left(-\frac{|Z|}{0.2}\right) \quad (1)$$

Respectively, R and Z are the Galacto-centric radius and the distance from the Galactic Plane in kpc; $R_\odot = 8.5$ kpc. The default model adopts α, $\beta = 1.25$, 3.56 based on the pulsar distribution (Strong et al. 2004), while the alternative model fits to a SNR distribution model described in Case & Bhattacharya (1998) and uses α, $\beta = 1.69$, 3.33. The two source distribution models are shown in Fig. 1 as a function of distance from Earth. Also overlaid in the figure for reference purposes is a corresponding curve derived from the 3D gas distribution obtained by Nakanishi & Sofue (2003, 2006).

4. Cosmic Ray Injection from Supernova Remnants

4.1. Injection of Protons and Primary Electrons

The standard theory of particle acceleration at SNRs through diffusive shock acceleration (DSA) predicts that the accelerated particles share a common non-thermal spectral shape when the gas density is not high ($n <$ a few cm^{-3}), apart from a high-energy cutoff or rollover for electrons around their maximum energy limited by radiative loss (e.g., Blasi et al. 2005; Ellison et al. 2007). As a result, we adopt a common spectral shape for the SNR-injected protons and primary electrons, except near the maximum energy where radiative loss introduces a spectral cutoff for the e^- spectrum.

We use a broken power-law injection spectrum for the SNR-injected primary CRs. The spectral parameters and injection luminosity of protons are chosen such that the propagated spectrum fits well with the observed CR proton flux at Earth. The e/p ratio, K_{ep}, is chosen such that the calculated total $e^- + e^+$ flux, which is mainly contributed by the 'SNR-propagation' and 'PWN-propagation' classes, reproduce the observed CR lepton spectrum measured by *Fermi* (Abdo et al. 2009a, 2010j) in the $50 - 150$ GeV energy band (more will be discussed in section 5). The adopted SS proton and electron injection spectra are shown in Fig. 2 and the relevant parameters are summarized in Table 3.

According to Yamazaki et al. (2006), the maximum electron energy is limited to ~ 14 TeV for SNRs older than 1 kyr, and ~ 7 TeV for those 10 kyr old; it then drops to ~ 0.5 TeV for ages of a few $\times$100 kyr. We calculate the loss-limited E_{max} in accordance with Yamazaki et al. (2006) (eqn. 2 and 10), assuming $B_d = 10$ μG, $r = 4$, $h = E_{51} = v_{i,9} = n_0 = 1$, and a hydro solution for a typical SNR lifetime of 50 kyr within the Sedov phase, such that:

$$E_{\rm max} = 13.8 \text{ TeV} \times \left(\frac{t_{\rm age}}{10 \text{ kyr}}\right)^{-\frac{3}{5}} \times \left(\frac{B_d}{10\ \mu\text{G}}\right)^{-\frac{1}{2}} \quad (2)$$

Beyond 50 kyr, the electron injection luminosity is expected to be too low to influence the time-averaged injection; hence, it is neglected in this study. The evolution of $E_{\rm max}$ of the continuously injected e^- from the Galactic ensemble of SNRs results in a smooth rollover of the calculated local e^- spectrum from the 'SNR-propagation' class at around 1 TeV. To determine the shape of the rollover, we use the simple propagation code described in the Appendix. This rollover is then applied to the propagated primary e^- spectrum calculated using GALPROP without the incorporation of $E_{\rm max}$ as described in detail in the Appendix.

4.2. Secondary Particles Contribution from SNRs

Secondary CRs are produced when the shock-accelerated nuclei interact with the surrounding gas. Blasi (2009) proposed that secondary positrons produced (and re-accelerated) in old SNRs may be responsible for the rise of the positron fraction observed by *PAMELA*. Meanwhile, antiprotons also should be produced and accelerated through an identical mechanism (Blasi & Serpico 2009). As of now, broad-band high-energy γ-ray spectra have been measured and published for 7 Galactic SNRs by *Fermi* and ground-based ACTs. Among them, 5 middle-aged SNRs are known to be interacting with local molecular clouds. Their γ-ray spectra are best explained by the decay of π^0 mesons (Abdo et al. 2009d, 2010a,d,h,i), with the underlying proton spectra at the interaction sites found to follow broken power-laws. A summary of the derived proton spectra for these γ-ray SNRs is given in Table 2. The γ-ray fluxes are found to be higher for middle-aged SNRs than younger ones, probably implying that the secondary CRs produced and injected by these interaction sites can be appreciable. However, the post-break indices of the deduced broken power-law proton spectra are generally soft (> 2.7), and particle acceleration in these interaction sites is probably inefficient beyond the break energies found around ~ 10 GeV (see Malkov et al. (2010) for possible theoretical interpretation). We try to estimate in our model the contribution of secondary CRs from these interaction sites to the fluxes at Earth (the 'SNR-cloud interaction' class), and deduce an upper limit for the total number of these sites in our Galaxy using constraints from updated CR measurements.

The injection luminosity of these secondary CRs is determined by the underlying proton spectrum and the product $n \times W_p$, where n and W_p are the average gas density and the total kinetic energy of CR protons, within each interaction site. With only a relatively small sample of this source class available, our knowledge on these quantities is very limited. With reference to γ-ray observations of SNRs interacting with clouds (Table 2), we adopt a typical $n \times W_p$ ($T_p > 1$ GeV) of 5×10^{51} erg cm^{-3} for each site. For this 'SNR-cloud interaction' source class, we use the same spatial distribution (Section 3), underlying proton spectrum, and propagation parameters as those adopted in the 'SNR-propagation' source class. Instead of using GALPROP, we use the simple

propagation code described in the Appendix to propagate the secondary particles produced, such that the injection luminosities per interaction site and the non-power-law injection spectra can be accommodated. In the code, neither re-acceleration effect nor hadronic interaction along the CR propagation path are considered.

5. Electron and Positron Spectra Injected from PWNe

Electrons and positrons are accelerated in the magnetosphere of a pulsar, injected to its associated PWN, and then accelerated again, presumably through diffusive shock acceleration at a termination shock. Electromagnetic spectra in the keV and MeV bands are mostly believed to originate from synchrotron radiation by the accelerated leptons, while those in the GeV and TeV bands are due to IC by the same lepton population. Until recently the Crab nebula was the only PWN detected clearly in both the GeV and TeV bands, and little was known about evolution of γ-ray emission from PWNe. In the past few years, however, *HESS* has detected several PWNe (Aharonian et al. 2006b; Gallant 2007; Funk 2007) shedding light to the evolution of their broadband emission (de Jager & Djannati-Ataï 2008; Mattana et al. 2009). Mattana et al. (2009) list 14 TeV PWNe of which *Fermi* has detected GeV emission from Crab, Vela X and MSH 15-52 (Abdo et al. 2010b,e,g). Of particular importance is that *HESS* has detected TeV emission from 3 PWNe whose ages are estimated to be greater than 50 kyr. This suggests that PWNe retain TeV leptons up to or longer than $\sim 10^5$ yr.

Zhang et al. (2008), Gelfand et al. (2009), Tanaka & Takahara (2010) and Bucciantini et al. (2010) have constructed dynamical evolution models of non-thermal emission in PWNe. Zhang et al. (2008) and Qiao et al. (2009) have applied their evolution model to 5 TeV PWNe (Crab Nebula, MSH 15−52, HESS J1825−137, Vela X and PWN G0.9+0.1). The particle spectra in these 5 PWNe can be approximated by broken power-law shapes with a break around $100 - 500$ GeV (see Table 1). Tanaka & Takahara (2010) used the broadband spectrum of Crab to calibrate their evolution model, and found that a fast decaying magnetic field ($\sim t^{-1.5}$) and a slowly evolving lepton spectrum can possibly explain the trend of increasing TeV γ-rays to X-ray ratio with age as implied by multi-wavelength observations of PWNe. The underlying lepton spectra predicted by these evolution models for the 5 PWNe observed in the TeV band are summarized in Table 1.

To construct the SS injection spectrum of primary e^- and e^+ from the PWNe ensemble, we first take the average of the spectra derived for the 5 observed γ-ray PWNe, weighted by their CR luminosities, to determine the spectral shape. The SS injection luminosity is renormalized jointly with the K_{ep} parameter of the 'SNR-propagation' class to reproduce the absolute lepton flux and spectral shape measured by *Fermi* (Abdo et al. 2009a, 2010j) in the $50 - 150$ GeV band, which is sufficient for us to uniquely determine the two normalizations. Fig. 3 shows the SS injection spectrum together with the spectra derived for the 5 γ-ray PWNe. The adopted injection parameters are summarized in Table 3.

We note that taking the simple average of the spectra derived from the very small sample of 5 observed γ-ray PWNe may not represent the SS injection spectrum from the Galactic ensemble of PWNe well. It is hence necessary to estimate the uncertainty of the adopted injection spectrum, which can contribute significantly to the systematic uncertainty of the calculations of positron fraction. Guided by the measurement data and modeling results given in Table 1, we constructed a series of representative injection spectra to sample the possible range of error: the spectral break energy is sampled in the $100 - 500$ GeV range, and the pre-break and post-break power-law indices are varied in the $1.0 - 1.7$ and $2.9 - 3.1$ ranges respectively. The resulted series of propagated CR spectra are each normalized to the *Fermi* lepton data as before, of which the extrema are taken to represent the systematic uncertainty.

6. Results and Discussion

The primary and secondary CR spectra obtained for the three source classes described in section 2 are summed and compared with the available CR observations at Earth and γ-ray observation by *Fermi*. In the figures, we show the calculated results using the default model parameters by the solid black lines, and their estimated systematic uncertainties by gray bands. The sensitivity of the results to the alternative setups − a different Galaxy halo size and a different source distribution − will be discussed below.

Anti-proton spectrum and fraction - The $\bar{p}$ spectrum and $\bar{p}/p$ ratio predicted by the model are found to be consistent with measurements by *PAMELA* and other experiments in Figs. 4 and 5 respectively. The 'SNR-cloud interaction' class along with the 'SNR-propagation' component contribute to the $\bar{p}$ intensity with similar spectral shapes. Using the latest measurements of the $\bar{p}$ spectrum by *PAMELA*, especially above 10 GeV, it is possible to obtain a crude upper limit on the total number of SNRs interacting with molecular clouds in the Galaxy. The upper limit is estimated to be ~ 200, given the assumed source distribution, underlying proton spectrum, and $n \times W_p$. In Figs. 4 and 5, contributions from a total of 200 interaction sites are shown for illustration. Future high-precision measurements of the $\bar{p}$ spectrum and $\bar{p}/p$ ratio, for example, by $AMS-02$ (AMS-02 Group 2009), as well as γ-ray observations of more SNR-cloud interaction systems by *Fermi* and ACTs will provide further constraints on the contributions from these secondary CR sources.

Electron + positron (lepton) spectrum - We see in Fig. 6 that our model agrees with the observed lepton spectrum reasonably well above ~ 20 GeV, within the estimated systematic uncertainty. A majority of the CR lepton flux is made up by the SNR-injected primary e^- which, however, comes short of reproducing the observation data at higher energies; in particular, the points measured by *Fermi* (Abdo et al. 2010j). The PWN-injected leptons fill up this gap and dominate at the higher energies, bringing the total spectrum back to agreement with the observed flux. The key for the reproduction of the lepton data is the break energy of the PWN injection spectrum at a few hundred GeV. The contributions from the SNR-cloud interaction sites is constrained by the upper limit estimated above from the $\bar{p}$ spectrum, and is found to be almost negligible

relative to the total spectrum at all energies. The calculated lepton flux from 200 SNR-cloud interaction sites is shown in Fig. 6 for illustration. In terms of the total lepton energy budget in the Galaxy above 1 GeV, contributions from 'PWN-propagation' class and SNR-cloud interaction sites make up only about 2 % while the 'SNR-propagation' class is responsible for the remaining 98 %.

Below $\sim$ 20 GeV, a discrepancy is found between the measured lepton spectrum and the model. CR spectra in this energy regime are known to be strongly affected by the heliospheric modulation (e.g., Shikaze et al. 2007), and the inaccuracy of the force-field approximation applied (Gleeson & Axford 1968) can be partially responsible for the disagreement. We do not observe, however, such a large discrepancy with measurements of the CR p and $\bar{p}$ spectra, which would have been affected by the same modulation effect. Although we can not rule out completely the modulation effect as the cause of this discrepancy, we will explore an alternative possibility later.

Positron fraction - One general feature predicted by our model is an enhancement of the positron fraction above $\sim$ 10 GeV (Fig. 7), as was recently observed by the *PAMELA* experiment. This enhancement is found to be closely related to the hard broken power-law spectrum of the PWN-injected leptons. Without the e^+ contribution from the Galactic PWN ensemble, the 'SNR-propagation' source class predicts a strictly decreasing positron fraction with energy in contradiction to the *PAMELA* points. Injection of secondary e^+ from the SNR-cloud interaction sites may boost the positron fraction by < 15 % for all energies, but is obviously insufficient to reproduce the 'enhancement' implied by *PAMELA* . At lower energies, the model shows good agreement with data, taking into consideration the large spread among the available measurements below a few GeV. The fractions measured by *PAMELA* in the $1-4$ GeV energy range are systematically lower than other measurements. Charge-sign dependent solar modulation effects (e.g. a smaller effective potential for e^- than e^+) have been suggested to be a possible resolution (e.g., Gast & Schael 2009), but we will not pursue this scenario any further in this study. The large systematic uncertainty estimated above 100 GeV mainly arises from the poorly constrained break energy of the PWN injection spectrum, which is seen to vary roughly in the broad range of $100-500$ GeV.

We found that positrons injected by the Galactic ensemble of PWNe play a central role in reproducing the observed positron fraction enhancement. There is however a possibility that only PWNe lying within a few 100 pc from Earth are significant in contributing to the e^+ flux. We use the propagation code described in the Appendix to estimate this local contribution from sources with distance-to-Earth less than 300 pc, with the same continuous source distribution adopted in our default GALPROP model. The calculation shows that these nearby PWNe make up less than 10% of the total calculated e^+ spectrum from the 'PWN-propagation' source class in the *PAMELA* energy band. In the SS picture of Galactic CR injection studied in this paper, PWNe beyond the local space explain most of the observed e^+ spectrum and fraction. This does not, however, rule out the possibility that a small fraction (up to $\sim$ 30 %) of the enhancement observed by *PAMELA* is due to non-SS injection from a few nearby PWNe, as already suggested in some recent papers (e.g., Grasso et al. 2009).

Possible low-energy electron component - A possible cause for the low-energy discrepancy of the lepton spectrum is that a class of CR sources (other than the presumed Galactic ensemble of SNRs and PWNe) may exist within a few 100 pc of Earth that contribute predominately low-energy e^-, but not e^+. We note that *Fermi* has found γ-ray emission from X-ray binaries (Abdo et al. 2009b,e) and *Suzaku* has found γ-ray pulsar-like periodic hard X-ray emission from a white dwarf (Terada et al. 2008) suggesting acceleration of electrons in its magnetosphere. Assuming the existence of such low-energy e^- sources, we add an ad-hoc power-law spectrum with an exponential cutoff to the calculated lepton spectrum as shown in the upper panel of Fig. 8. The positron fraction is naturally reduced accordingly as shown in the bottom panel. Since CR e^- with energy ~ 10 GeV propagate only a few 100 pc over 1 Myr, these speculative sources should be relatively close to Earth. However, it is in order to note that this low-energy discrepancy is a result of one of our assumptions that the injected protons and primary e^- from SNRs share a common injection spectral shape (for electron energies less than $E_{\rm max}$ in equation 2), which is supported by the standard DSA theory but have no direct observational evidence so far.

Gamma-ray spectrum - We compare in Fig. 9 the γ-ray spectrum calculated by our model for the $|b| > 10^\circ$ region in the Galaxy with that measured by *Fermi* (Abdo et al. 2010m), which serves as an additional consistency check. The contributions from the 3 source classes described in section 2 are shown separately. The total spectrum integrating over all source classes, γ-ray point sources from the 1st Fermi Catalog (Abdo et al. 2010f), and the isotropic background (extragalactic diffuse emission and residual CRs that were incorrectly classified as γ-rays) comes out consistent with the data within the statistical and systematic uncertainties.[5] Most of the observed flux is from the diffuse γ-rays produced by SNR-injected CRs along their propagation path, the isotropic background, and the point sources. Diffuse emission produced by the PWN-injected leptons is much less intense. Within the upper limit set for the total number of SNRs found from the high-energy $\bar{p}$ data to be interacting with clouds, γ-ray emission from the 'SNR-cloud interaction' class is found to be insignificant in this sky region sampled in Fig. 9 (contribution from 200 interaction sites are shown in the figure for illustration).

Alternative setups - Calculations performed for the default model are repeated for the two alternative models - one with a different source distribution (see section 3), and another with a larger Galaxy halo size of 10 kpc. The impacts of alternative setups on the results are summarized below. In general, the results can be reproduced almost exactly and our conclusions remain the same, provided that the appropriate model parameters are changed accordingly, as follows: For both alternative models, the injection luminosities of primary CRs for both 'SNR-propagation' and 'PWN-propagation' classes have to be slightly varied relative to those required by the default setup. The required percentage changes in the injection luminosities, as well as the resulting total

[5]It is not surprising that the γ-ray spectrum our model predicts is consistent with the *Fermi* observation because the GALPROP proton injection spectrum has already been tuned to reproduce the Galactic γ-ray spectrum. More rigorous tests will be done when large-scale Galactic diffuse emission data become available.

CR energy budget in the Galaxy, are summarized in Table 4. Most of the deviations are found to be within ±20 % of the default model. For the large-halo setup, a larger diffusion coefficient and a slightly weakened strength of re-acceleration in the ISM than the default are necessary to reproduce the observed B/C ratio. These changes are shown in Table 3. The γ-ray spectrum shown in Fig. 9 for the $|b| > 10^\circ$ sky region do not change appreciably among the three setups. More detailed comparison with large-scale γ-ray data, e.g., spectra from the Galactic ridge and the inner-Galaxy region, as well as small-scale structures, may make it possible to discriminate between the models and help put constraints on important quantities such as the halo size, gas, and source distributions of our Galaxy.

Energy budget of Galactic CR - With γ-ray observations of CR sources and measurements of charged CR spectra analyzed coherently under a common calculation platform using GALPROP, it is possible to extract a self-consistent set of quantities related to Galactic CRs, including the injected CR energies from SNRs and PWNe, interaction rate of nuclear CRs, and γ-ray emissivity in the Galaxy. These quantities depend mildly on the presumed boundary of the propagation volume and the assumed source distribution. The results are summarized in Table 4 and Table 5. Based on the calculated energetics, various useful quantitative information can be extracted as we demonstrate below for the default set of model parameters:

- From the total energy and luminosity given for primary protons in Table 4, we can roughly estimate the typical lifetime of CR protons ($T_p > 0.1$ GeV) inside the Galaxy as $\sim 7.5 \times 10^{55}/2.0 \times 10^{48} = 3.8 \times 10^7$ yr. A similar estimate for CR leptons injected by PWNe is roughly 9.1×10^6 yr, substantially shorter than for the protons. This mean lifetime is roughly consistent with the synchrotron loss time-scale of electrons with an energy of ~ 20 GeV (e.g., Yamazaki et al. 2006), close to the mean energy of leptons injected by the PWNe ensemble in our model. The difference in the lifetime becomes larger for CRs with $T > 1$ GeV: $\sim 4.6 \times 10^7$ yr for protons versus $\sim 6.9 \times 10^6$ yr for leptons.

- Approximating the CR proton spectrum in the Galaxy ($T_p > 1$ GeV) by a broken PL shape consistent with LIS ($E_b = 7$ GeV, $\gamma_1 = 2.0$, $\gamma_2 = 2.75$), we obtain the average kinetic energy per CR ($T_p > 1$ GeV) to be 3.5 GeV or 5.6×10^{-3} erg.

- For a typical lifetime of $\sim 4 \times 10^7$ yr, protons cross a column density of $4n \times 10^{25}\mathrm{cm}^{-2}$ where n is the number density of hydrogen atoms (cm^{-3}) averaged over the propagation volume bounded by $R_{max} = 20$ kpc and $Z_{max} = 4$ kpc. Since the *pp* inelastic cross-section is ~ 30 mb or $\sim 30 \times 10^{-27}$ cm^2, about $1 \times n$ of CRs interact with the ISM gas. Since the mean kinetic energy of protons is ~ 3.5 GeV, the π^0 multiplicity comes out to be ~ 0.5 (Kamae et al. 2005). Hence a CR proton produces, on average, $\sim 1 \times n$ pionic γ-rays in its life.

- For a total number of target H-atom of 1.1×10^{67} from H I, H_2 and H II regions given in Ferrière (2001) and the pionic γ-ray emissivity averaged over the default GALPROP cylindrical box, the number of pionic γ-rays ($E_\gamma > 1$ GeV) coming out of the Galaxy can be estimated

as $(4.5 \times 10^{-27}) \times (1.1 \times 10^{67}) = 5.0 \times 10^{40}$ s^{-1}. Since the total number of CR protons ($T_p > 1$ GeV) is estimated to be $6.1 \times 10^{55}/5.6 \times 10^{-3} = 1.1 \times 10^{58}$, the average number of pionic γ-rays ($E_\gamma > 1$ GeV) is $(5.0 \times 10^{40})/(1.1 \times 10^{58}) = 5 \times 10^{-18}$ s^{-1} per CR proton, or $(10^{15}) \times (5 \times 10^{-18}) = 5 \times 10^{-3}$ integrated over the typical lifetime of one CR proton of $\sim 10^{15}$ s. Hence, CR protons spend most of their lives on average propagating in a low-density medium, with $n \sim 0.005$ cm^{-3}, whereas the typical density of the 'SNR-cloud interaction' sites is ~ 100 cm^{-3}.

Because of the constraints given by the gamma-ray observations of the CR sources and by the CR proton and lepton flux measurements, these estimates vary by only ~ 20 % or less and provide a coherent picture of Galactic CR propagation.

The overall success of the model in reproducing the observed CR ratios and spectra suggests that the majority of the CRs observed at Earth are steadily injected from the Galactic ensembles of SNRs and PWNe. The consistency between the observed and predicted diffuse γ-ray spectra strengthens this interpretation.

7. Conclusion

The analysis presented here has connected the recent γ-ray observations of CR acceleration sites by *Fermi* and ACTs and the recent charged CR measurements at Earth in the common platform of GALPROP. We were able to do this by assuming all CR species in the Galaxy are in a steady state, on which GALPROP is built. CRs are assumed to be injected only from SNRs and PWNe with the spectra averaged over their respective evolution history. The sources are distributed, approximately proportional to, either the distribution of pulsars or SNRs in the Galacto-centric cylindrical coordinate system. Throughout the analysis we have not used the positron fraction either explicitly or implicitly to constrain the input parameters for GALPROP. The analysis has also remained totally blind to the measured $\bar{p}/p$ ratio. With these assumptions about the distributions, luminosities, and spectra of the sources (including secondary CRs produced in SNRs), the model reproduces the positron fraction observed by *PAMELA* reasonably well (Fig. 7) the $\bar{p}/p$ ratio by *PAMELA* (Fig. 5) very well under the constraint of the observed total $e^- + e^+$ spectrum (Fig. 6) [6].

We conclude that the energy dependence of the excess in the positron fraction can be considered, reasonably well, to be due to the contributions from the Galactic ensemble of PWNe and secondary e^+ produced by CR protons along their propagation path. The observed $\bar{p}$ flux is predominantly attributed to interactions of the primary nuclear CRs along their propagation paths, while those potentially injected from dense clouds interacting with middle-aged SNRs are estimated

[6] We note that our model inherits the GALPROP prediction on the $\bar{p}/p$ ratio except for the contribution from the SNR-cloud interaction.

to contribute less than ~ 11 % in total flux above 100 MeV. The SS contribution from local SNRs and PWNe (within 300 pc from Earth) is estimated to be less than ~ 10 % in the e^+ spectrum, which is not crucial for reproducing the observed positron fraction.

Assuming that the SN rate in the Milky Way is one in 30 years [7], and adopting the injection luminosity of primary CR protons from SNRs listed in Table 4 and SNRs' active life of 5×10^4 yr, we estimate that ~ 1700 SNRs are actively injecting CRs into the ISM, and each SNR injects $\sim 6.1 \times 10^{49}$ erg of CRs ($E > 0.1$ GeV) into the Galactic space in its lifetime. Our result implies that for a typical $n \times W_p$ ($T_p > 1$ GeV) of 5×10^{51} erg cm^{-3}, up to ~ 200 of them can be interacting with dense clouds (section 6). Similarly, if we assume a PWN birth rate of one in 50 years and that PWNe remain active for 10^5 yr on average, ~ 2000 PWNe are injecting CR leptons, with each PWN injecting $\sim 7.2 \times 10^{46}$ erg of CR leptons into the Galactic space. CR protons with $T_p > 1$ GeV stay $\sim 4.6 \times 10^7$ yr in the Galaxy with only 0.1% interacting with gas while CR leptons with $T_e > 1$ GeV lose energy in $\sim 6.9 \times 10^6$ yr.

A discrepancy is found in the low energy electron spectrum below ~ 20 GeV. If the corrections for the solar modulation effect are well approximated to the measured spectra, it can imply that an additional class of local CR sources which preferentially inject low-energy ($E < 20$ GeV) electrons is required.

Our results on the energy budget of Galactic CR are in general agreement with those recently published by Strong et al. (2010). One major difference is in the injection spectrum of the primary electrons: they assumed a broken power-law spectrum with a much harder index for the lower energy component (-1.60 instead of -1.98) and a substantially lower break energy (4 GeV instead of 7 GeV). A few other GALPROP parameters are different but no more than ~ 15 %. The CR luminosity listed under the Models 2 and 3 of Diffusive Reacceleration in their Table 2 can be compared with the luminosity listed in the left-most (default) and Alt Model II columns in our Table 4. Their CR luminosity is $\sim 11 - 12$ % higher for primary protons and ~ 8 % lower for primary electrons than ours, both within accuracy of CR energetics study at this time.

Higher precision γ-ray spectra expected from *Fermi* as well as precision measurements of the positron fraction above 100 GeV and the lepton spectrum in the TeV range by $AMS-02$ (AMS-02 Group 2009) will allow us to extract important information on the evolution of PWNe and SNRs. *Fermi* will soon measure anisotropy in the γ-ray emissivity at nearby molecular clouds, and either detect or exclude the proposed GRB scenario for the *PAMELA* e^+ excess (Fujita et al. 2009; Perrot & Grenier 2003). Future high precision measurement of $\bar{p}$ by $AMS-02$ (AMS-02 Group 2009) will further constrain contribution from the SNR-cloud interaction sites.

Acknowledgment

[7] Diehl et al. (2006) estimate the rate of core-collapse supernovae to be $\sim 1.9 \pm 1.1$ per century. The Type Ia supernovae rate is less constrained observationally, ranging from $0.3 - 1.1$ per century (e.g. Mannucci et al. 2005; Knödlseder et al. 2005). These two rates add up to ~ 3 per century.

We have benefitted greatly from question-and-answer sessions with I. Moskalenko and A. Strong in understanding the GALPROP code for which we are very grateful. We thank R. Yamazaki, F. Takahara and S. Tanaka for kindly answering our inquiries about their work on electron spectra in SNRs and PWNe. The Fermi LAT collaboration members, especially M. Ackermann, J.-M. Casandijan, S. Digel, G. Jóhannesson, T. Mizuno, J. Ormes, and L. Tibaldo helped us in clarifying various issues related to the diffuse gamma-ray emission and improving the paper. We also acknowledge discussion with J. Arons, D. Ellison, V. Petrosian, and L. Stawarz for discussion on the theoretical aspect of the paper.

As members of the *Fermi* LAT Collaboration, we acknowledge generous ongoing support from a number of agencies and institutes that have supported both the development and the operation of the LAT as well as scientific data analysis. These include the National Aeronautics and Space Administration and the Department of Energy in the United States, the Commissariat à l'Energie Atomique and the Centre National de la Recherche Scientifique / Institut National de Physique Nucléaire et de Physique des Particules in France, the Agenzia Spaziale Italiana and the Istituto Nazionale di Fisica Nucleare in Italy, the Ministry of Education, Culture, Sports, Science and Technology (MEXT), High Energy Accelerator Research Organization (KEK) and Japan Aerospace Exploration Agency (JAXA) in Japan, and the K. A. Wallenberg Foundation, the Swedish Research Council and the Swedish National Space Board in Sweden.

Additional support for science analysis during the operations phase is gratefully acknowledged from the Istituto Nazionale di Astrofisica in Italy and the Centre National d'Études Spatiales in France.

A. Appendix

Models described in this study are primarily built using GALPROP as much as possible. Calculations that cannot be readily implemented in a typical GALPROP model are accomplished via a simple propagation code separately developed by us, which include the following: (1) the local contribution of CR positrons from PWNe lying within a given distance from Earth; (2) contribution of secondary particles injected from SNRs interacting with clouds; and (3) the high-energy rollover inherent to the primary e^- spectrum injected from SNRs due to spectral cutoff at a time-dependent maximum energy. To obtain the CR spectra propagated from a continuous source distribution characterized by distance-to-Earth $\boldsymbol{r}$, source age $t_{\rm age}$, and the active lifetime of each source $t_{\rm life}$ (time interval during which CRs are injected into the ISM from a source), we use the analytic solution of the simple diffusion-loss transport equation adapted from Atoyan et al. (1995) [8]:

[8]This propagation calculation does not include re-acceleration effect and interaction involving heavy nuclei which can possibly affect the B/C ratio.

$$N(E,\boldsymbol{r}) = \int_{t_{\rm age}-t_{\rm life}}^{t_{\rm age}} \frac{Q_{\rm inj}(E_i,\boldsymbol{r},t')b(E_i)}{\pi^{3/2}b(E)r_{\rm D}^3(E,t')} e^{-(|\boldsymbol{r}|/r_{\rm D}(E,t'))^2} dt' \tag{A1}$$

$$r_{\rm D}(E,t) \approx 2\sqrt{D(E)\frac{1-(1-b_0Et)^{1-\delta}}{(1-\delta)b_0Et}} \tag{A2}$$

Here $b(E)$ is the energy-loss rate of the CRs, which can be expressed as $b(E) \approx b_0E^2$ for synchrotron and IC losses of leptons during propagation, while loss is considered negligible for nuclei (such that equations A1 and A2 reduce to the usual solution of a simple 1-D diffusion equation and diffusion length respectively). E_i is the initial injection energy of CRs whose observed energy at Earth is E. The effective diffusion length $r_{\rm D}(E,t)$ for a particle with observed energy E and propagation time t is given by equation A2, in which the energy loss effect is accounted for. $D(E) \propto \beta E^\delta$ is the adopted spatial diffusion coefficient, where the index $\delta = 1/3$ is used consistent with the GALPROP calculations. The CR injection term is given by $Q_{\rm inj}(E,\boldsymbol{r},t) = Q(E,t)n_{\rm soc}(\boldsymbol{r},t)$ where $Q(E,t)$ is the injection spectrum and $n_{\rm soc}(\boldsymbol{r},t)$ is the source distribution in space-time. The spatial distribution of sources is the same as the distribution used in the default GALPROP model, while $t_{\rm age}$ of the sources are assumed to be distributed uniformly in time starting from a maximum of 10^8 yr ago up to 5×10^4 yr ago. For every source, $t_{\rm life}$ is assumed to be 5×10^4 yr.

For (1), the injection spectra and luminosities of e^+ and e^- are directly taken from the GALPROP inputs and outputs adopted for the 'PWN-propagation' class of the default model (see Tables 3 and 4). For (2), these are calculated for the secondary e^+, e^- and $\bar{p}$ according to the description in Section 4.2. Tertiary CRs produced through hadronic interactions during propagation of $\bar{p}$ in the ISM are neglected. For (3), a time-dependent exponential cut-off is applied to the injection term for the SNR-injected primary e^- ($Q(E,t) \propto e^{-E/E_{\rm max}(t)}$) to incorporate the time-evolving maximum electron energy $E_{\rm max}(t)$ given by equation 2. This results in a smooth high-energy turnover of the propagated primary e^- spectrum at Earth, which occurs at around 1 TeV. This calculated turnover is then applied to the GALPROP-calculated primary e^- spectrum from the 'SNR-propagation' source class.

REFERENCES

Abdo, A. A., et al. 2009a, Physical Review Letters, 102, 181101

Abdo, A. A., et al. 2009b, ApJ, 701, L123

Abdo, A. A., et al. 2009c, ApJ, 703, 1249

Abdo, A. A., et al. 2009d, ApJ, 706, L1

Abdo, A. A., et al. 2009e, ApJ, 706, L56

Abdo, A. A., et al. 2009f, Science, 326, 1512

Abdo, A. A., et al. 2009g, Physical Review Letters, 103, 251101

Abdo, A. A., et al. 2010a, Science 327, 1103

Abdo, A. A., et al. 2010b, ApJ, 708, 1254

Abdo, A. A., et al. 2010c, ApJ, 710, L92

Abdo, A. A., et al. 2010d, ApJ, 712, 459

Abdo, A. A., et al. 2010e, ApJ, 713, 146

Abdo, A. A., et al. 2010f, ApJS, 187, 460

Abdo, A. A., et al. 2010g, ApJ, 714, 927

Abdo, A. A., et al. 2010h, ApJ, 718, 348

Abdo, A. A., et al. 2010i, ApJ, submitted

Abdo, A. A., et al. 2010j, submitted to PRL.

Abdo, A. A., et al. 2010k, in preparation.

Abdo, A. A., et al. 2010l in preparation.

Abdo, A. A., et al. 2010m, Phys. Rev. Lett., 104, 10

Acciari, V. A., et al. 2009, ApJ, 698, L133

Acciari, V. A., et al. 2010, ApJ, 714, 163

Adriani, O., et al. 2009, Nature, 458, 607

Adriani, O., et al. 2009, Physical Review Letters, 102, 051101

Aharonian, F. A., Atoyan, A. M., & Voelk, H. J. 1995, A&A, 294, L41

Aharonian, F. A., et al., 2005a, A&A, 435, L17

Aharonian, F. A., et al., 2005b, A&A, 437, L7

Aharonian, F. A., et al., 2005c, A&A, 442, L25

Aharonian, F., et al. 2006a, A&A, 448, L43

Aharonian, F. A., et al., 2006b, ApJ, 637, 777

Aharonian, F. A., et al., 2006c, A&A, 448, L43

Aharonian, F. A., et al., 2006d, A&A, 449, 223

Aharonian, F. A., et al., 2006e, A&A, 460, 365

Aharonian, F. A., et al., 2007, A&A, 464, 235

Aharonian, F., et al. 2008a, Physical Review Letters, 101, 261104

Aharonian, F., et al. 2008b, A&A, 481, 401

Aharonian, F., et al., 2009, A&A, 508, 561

Ahlers, M., Mertsch, P., & Sarkar, S. 2009, Phys. Rev. D, 80, 123017

Alberi, G., & Goggi, G. 1981, Phys. Reports, 74, 1

Albert, J., et al. 2007a, ApJ, 664, L87

Albert, J., et al. 2007b, A&A, 474, 937

http://ams-02project.jsc.nasa.gov/html/Projectpage.htm

Atoyan, A. M., Aharonian, F. A., & Voellk, H. J. 1995, Phys. Rev. D, 52, 3265

Anticic, T., et al. 2010, European Physical Journal C, 65, 9

Bergström, L., Edsjö, J., & Ullio, P. 1999, ApJ, 526, 215

Biermann, P. L., et al. 2009, Physical Review Letters, 103, 061101

Blasi P., Gabici S., & Vannoni G. 2005, MNRAS, 361, 907

Blasi, P. 2009, Physical Review Letters, 103, 051104

Blasi, P., & Serpico, P. D. 2009, Physical Review Letters, 103, 081103

Blattnig, S. R., Swaminathan, S. R., Kruger, A. T., Ngom, M., & Norbury, J. W. 2000, Phys. Rev. D, 62, 094030

Boezio, M., et al. 2009, New Journal of Physics, 11, 105023

Bucciantini, N., Arons, J., & Amato, E. 2010, arXiv:1005.1831

Case, G. L. & Bhattacharya, D. 1998, ApJ, 504, 761

Chang, J., et al. 2008, Nature, 456, 362

de Jager, O. C., & Djannati-Ataï, A. 2008, arXiv:0803.0116

Delahaye, T., Lavalle, J., Lineros, R., Donato, F., & Fornengo, N. 2010, arXiv:1002.1910

Diehl, R., et al. 2006, Nature, 439, 45

Ellison D.C., et al. 2007, ApJ, 661, 879

Ferrière, K. M. 2001, Reviews of Modern Physics, 73, 1031

Available from http://fermi.gsfc.gov/ssc/data/access/lat/BackgroundModels.html.

Fiasson, A., et al. (the HESS collaboration) 2009, in Proceedings of the 31st International Cosmic Ray Conference

Fujita, Y., Kohri, K., Yamazaki, R., & Ioka, K. 2009, Phys. Rev. D, 80, 063003

Funk, S. 2007, Ap&SS, 309, 11

Gaensler, B. M., & Slane, P. O. 2006, ARA&A, 44, 17

Gaisser, T. K., & Schaefer, R. K. 1992, ApJ, 394, 174

Gallant, Y. A. 2007, Ap&SS, 309, 197

Gast, H., & Schael S. 2009, Proceedings of the 31st International Cosmic Ray Conference (2009, Lodz) O.G.1.3

Gelfand, J. D., Slane, P. O., & Zhang, W. 2009, ApJ, 703, 2051

Gleeson, L. J., & Axford, W. I. 1968, ApJ, 154, 1011

Grasso, D., et al. 2009, Astroparticle Physics, 32, 140

Ioka, K. 2010, Progress of Theoretical Physics, 123, 743

Kamae, T., Abe, T., & Koi, T. 2005, ApJ, 620, 244

Kamae, T., Karlsson, N., Mizuno, T., Abe, T., & Koi, T. 2006, ApJ, 647, 692

Katz, B., Blum, K., Morag, J., & Waxman, E. 2010, MNRAS, 547

Kawanaka, N., Ioka, K., & Nojiri, M. M. 2010, ApJ, 710, 958

Knödlseder, J., et al. 2005, A&A, 441, 513

Kobayashi, T., Komori, Y., Yoshida, K., & Nishimura, J. 2004, ApJ, 601, 340

Lallement, R., et al. 2003, A&A, 411, 447

Malkov, M. A., Diamond, P. H., & Sagdeev, R. Z. 2010, arXiv:1004.4714

Mattana, F., et al. 2009, ApJ, 694, 12

Malyshev, D., Cholis, I., & Gelfand, J. 2009, Phys. Rev. D, 80, 063005

Mannucci, F., et al. 2005, A&A, 433, 807

Meade, P., Papucci, M., Strumia, A., & Volansky, T. 2010, Nuclear Physics B, 831, 178

Mertsch, P., & Sarkar, S. 2009, Physical Review Letters, 103, 081104

Mori, M. 1997, ApJ, 478, 225

Moskalenko, I. V., Strong, A. W., Ormes, J. F., & Potgieter, M. S. 2002, ApJ, 565, 280

Moskalenko, I. V., & Strong, A. W. 1998, ApJ, 493, 694

Nakanishi, H., & Sofue, Y. 2003, PASJ, 55, 191

Nakanishi, H., & Sofue, Y. 2006, PASJ, 58, 847

Perrot, C. A. & Grenier, I. A., 2003, A&A, 404, 519

Profumo, S. 2008, arXiv:0812.4457

Ptuskin, V. S., & Zirakashvili, V. N. 2003, A&A, 403, 1

Ptuskin, V. et al. 2006, ApJ, 642, 902

Qiao, W. F., et al. 2009, Research in Astronomy and Astrophysics, 9, 449

Shikaze, Y., et al. 2007, Astroparticle Physics, 28, 154

Stawarz, Ł., Petrosian, V., & Blandford, R. D. 2010, ApJ, 710, 236

Strong, A. W., Moskalenko, I. V., & Reimer, O. 2004, ApJ, 613, 962

Strong, A. W., Moskalenko, I. V., & Ptuskin, V. S. 2007, Annual Review of Nuclear and Particle Science, 57, 285

Strong, A. W., Porter, T. A., Digel, S. W., Jóhannesson, G., Martin, P., Moskalenko, I. V., Murphy, E. J., & Orlando, E. 2010, ApJ, 722, L58

1 Tan, L. C. & Ng, L. K., 1982 Phys. Rev. D26, 1179

2 Tan, L. C. & Ng, L. K., 1983a J. Phys. G9, 227

3 Tan, L. C. & Ng, L. K., 1983b J. Phys. G9, 1289

4 Tanaka, S. J., & Takahara, F. 2010, ApJ, 715, 1248

5 Terada, Y., et al. 2008, PASJ, 60, 387

6 Yamazaki, R., et al. 2006, MNRAS, 371, 1975

7 Yüksel, H., Kistler, M. D., & Stanev, T. 2009, Physical Review Letters, 103, 051101

8 Zhang, L., et al. 2008, ApJ, 676, 1210

Table 1. Five PWNe observed by *Fermi* and ACTs

Source Name	Age kyr	Distance kpc	Detection ACTs	Detection *Fermi*	Broken Power-law [a] E_{br}[GeV]	α_{LE}	α_{HE}	L_e [b] 10^{37} erg/s	Refs. [c]
Crab	1.0	2.0	yes	yes	300	1.5	3.1	46	[d]
MSH 15-52	1.7	5.0	yes	yes	460	1.5	2.9	1.8	[e]
HESS J1825-137	21	3.9	yes	no	120	1.0	2.9	0.9	[f]
Vela X	11	0.29	yes	yes	100	1.9	2.1	0.04	[g]
G0.9+0.1	6.5	8.5	yes	no	80	1.7	2.9	3.5	[h]

[a]Effective spectra of lepton injected by the PWNe into the Galactic space, approximated by broken power-law shape. Injection model for the Crab Nebula is taken from Tanaka & Takahara (2010), and that for MSH 15-52 from Abdo et al. (2010g); Zhang et al. (2008). The rest are from Zhang et al. (2008) and Qiao et al. (2009).

[b]The lepton injection luminosity is calculated on the current spin-down luminosity of the driving pulsar, and the fraction of power channeled to magnetic energy.

[c]References for ages and distances are found in the literatures cited below.

[d]Abdo et al. (2010b); Tanaka & Takahara (2010); Zhang et al. (2008) and references therein.

[e]Abdo et al. (2010g); Aharonian et al. (2005a); Zhang et al. (2008)

[f]Aharonian et al. (2005c, 2006e); Zhang et al. (2008)

[g]Abdo et al. (2010e); Aharonian et al. (2006d); Qiao et al. (2009)

[h]Qiao et al. (2009)

Table 2. Seven SNRs observed by *Fermi* and ACTs

SNR Name	Age kyr	Distance kpc	Gas dens × CR [a] $n \times W_p$[erg cm^{-3}]	PL or Broken-PL [b] E_{br}[GeV]	α_{LE}	α_{HE}	Refs. [c]
Cas A	0.3	3.4	$(3.2 - 3.8) \times 10^{50}$	–	$2.1 - 2.3$	–	[d]
RX J1713.7−3946	1.6	~ 1.0	$\sim 1 \times 10^{50}$	–	1.7	–	[e]
W49B	4.0	7.5	1.1×10^{52}	4.0	2.0	2.7	[f]
W44	20	3.0	6×10^{51}	8.0	1.74	3.7	[g]
W51C	30	6.0	5.2×10^{51}	15	1.5	2.9	[h]
IC 443	30	1.5	1.3×10^{51}	69	2.09	2.87	[i]
W28	40	2.0	2.4×10^{51}	–	2.7	–	[j]

[a]Product of the average gas density and the total kinetic energy of CR protons in the SNR-cloud interaction site. Errors associated with these estimations are likely to be within a factor less than 10 above and below.

[b]For protons interacting with dense clouds at SNRs. PL stands for a power-law spectrum.

[c]References for ages and distances are found in the literatures cited below.

[d]Abdo et al. (2010c); Albert et al. (2007b); Acciari et al. (2010)

[e]Abdo et al. (2010k); Aharonian et al. (2005b, 2006d, 2007)

[f]Abdo et al. (2010i)

[g]Abdo et al. (2010a)

[h]Abdo et al. (2009d); Fiasson et al. (2009)

[i]Abdo et al. (2010d); Albert et al. (2007a); Acciari et al. (2009)

[j]Abdo et al. (2010h); Aharonian et al. (2008b)

Table 3. Summary of Model Parameters

Parameter	Value	Description
GALPROP Inputs		
B	$8 \times \exp\left(\frac{R_\odot - R}{50}\right) \times \exp\left(-\frac{\lvert Z\rvert}{3}\right)$ μG	B-field model in ISM [a]
D	$(5.8 - 10.0) \times 10^{28} \beta$ $(\frac{\mathrm{R}}{4\mathrm{GV}})^{0.33}$ cm^{2}s^{-1}	Diffusion coefficient [b]
v_A	$(30 - 24.2)$ km s^{-1}	Alfvén wave velocity in ISM [b]
$Z_{\max}$	$(4 - 10)$ kpc	Galactic half-halo size [b]
Galactic Ensemble of Supernova Remnants [c]		
$L_{p,\ >0.1\mathrm{GeV}}$	6.42×10^{40} erg s^{-1}	Total luminosity of proton
$L_{e,\ >0.1\mathrm{GeV}}$	1.23×10^{39} erg s^{-1}	Total luminosity of primary e^-
K_{ep}	0.02	The e/p ratio
E_b	7 GeV	Spectral break energy
γ_1	2.0	Spectral index below E_b
γ_2	2.5	Spectral index above E_b
$n \times W_{p,\ >1\mathrm{GeV}}$	5×10^{51} erg cm^{-3}	See footnote a in Table 2
Galactic Ensemble of Pulsar Wind Nebulae [c]		
$L_{e,\ >0.1\mathrm{GeV}}$	4.56×10^{37} erg s^{-1}	Total luminosity of $e^+ + e^-$
E_b	300 GeV	Spectral break energy
γ_1	1.5	Spectral index below E_b
γ_2	3.1	Spectral index above E_b

[a] R and Z are Galactocentric distances in kpc.

[b] The first value is for $Z_{\max} = 4$ kpc and the second for 10 kpc.

[c] Quoted luminosities and K_{ep} correspond to the default setup with $Z_{\max} = 4$ kpc, $R_{\max} = 20$ kpc, and the default spatial source distribution.

Table 4. Energetics of Galactic Cosmic Rays in the Steady State [a]

Particle	$T_p > 0.1$ (1.0) GeV [erg] or [erg s^{-1}]	Alt. Model I [b] Δ in %	Alt. Model II [c] Δ in %
K.E. of CRs injected by SNRs integrated in the SS Galaxy [d]			
p	7.5×10^{55} (6.1×10^{55})	+14.8 %	n/a
e^- (pri)	1.9×10^{54} (7.4×10^{53})	+9.3 %	n/a
e^- (sec)	1.7×10^{53} (5.2×10^{52})	+1.8 %	n/a
e^+	6.9×10^{53} (1.5×10^{53})	+1.5 %	n/a
$\bar{\mathrm{p}}$	4.4×10^{51} (4.4×10^{51})	−0.5 %	n/a
Injection luminosity of CRs from SNRs			
p	6.4×10^{40} (4.2×10^{40})	+14.6 %	−6.5 %
e^- (pri)	1.2×10^{39} (8.0×10^{38})	+4.1 %	+21.1 %
K.E. of CRs injected by PWNe integrated in the SS Galaxy [d]			
e^-	6.6×10^{51} (4.8×10^{51})	+9.2 %	n/a
e^+	6.6×10^{51} (4.8×10^{51})	+9.2 %	n/a
Injection luminosity of CRs from PWNe			
e^-	2.3×10^{37} (2.2×10^{37})	+0.7 %	+19.1 %
e^+	2.3×10^{37} (2.2×10^{37})	+0.7 %	+19.1 %

[a]The results listed here are extracted from the GALPROP outputs for our models.

[b]Model using the alternative source distribution (see Section 3)

[c]Model using a larger half-halo size of $Z_{\max} = 10$ kpc.

[d]Kinetic energy of the accumulated CRs within the assumed boundary of the Galaxy. Models with different propagation volumes are not compared.

Table 5. π^0-decay γ-ray emissivities in different regions of the Galaxy [a]

Region	$E_\gamma > 0.1$ GeV $[\mathrm{s}^{-1}\mathrm{H}^{-1}]$	$E_\gamma > 1.0$ GeV $[\mathrm{s}^{-1}\mathrm{H}^{-1}]$	Alt. Model I [b] Δ in %	Alt. Model II [c] Δ in %
$R < 4.25$ kpc, $\lvert Z\rvert < 100$ pc	2.9×10^{-25}	3.5×10^{-26}	-28.9 %	-16.4 %
$R < 10$ kpc, $1.5 < \lvert Z\rvert < 3$ kpc	9.4×10^{-26}	1.1×10^{-26}	-10.8 %	$+42.1$ %
Whole Galaxy	3.8×10^{-26}	4.5×10^{-27}	$+10.2$ %	$+13.1$ %

[a]The results listed here are extracted from the GALPROP outputs for our models.

[b]Model using the alternative source distribution (see Section 3)

[c]Model using a larger halo size of $Z_{\mathrm{max}} = 10$ kpc.

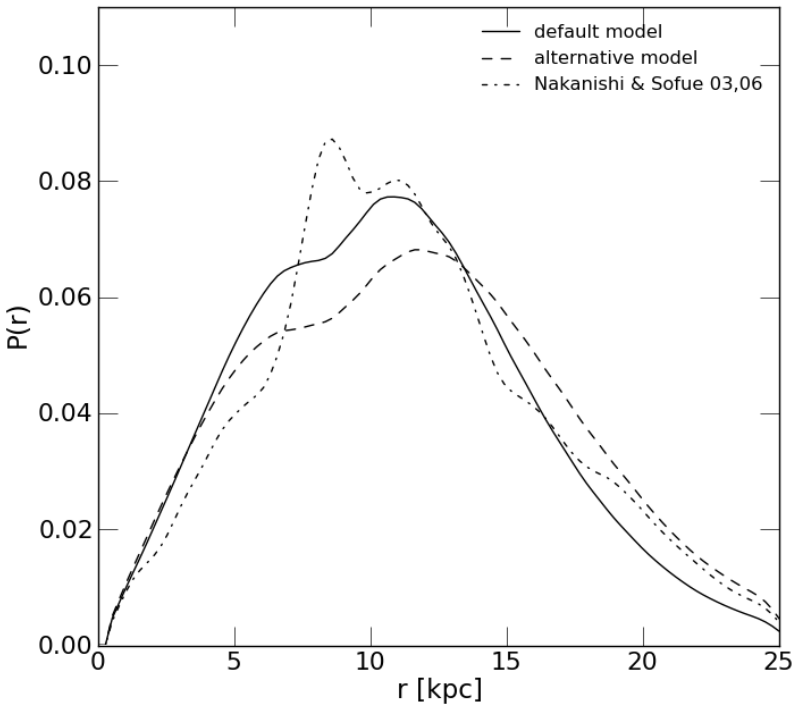

Fig. 1.— Probability density of source distribution plotted as a function of distance from Earth: the parametric model in GALPROP with the default (solid) and alternative model (dash) parameters. The corresponding curve derived from the 3D gas distribution obtained by Nakanishi & Sofue (2003, 2006) is also shown as a dash-dotted line.

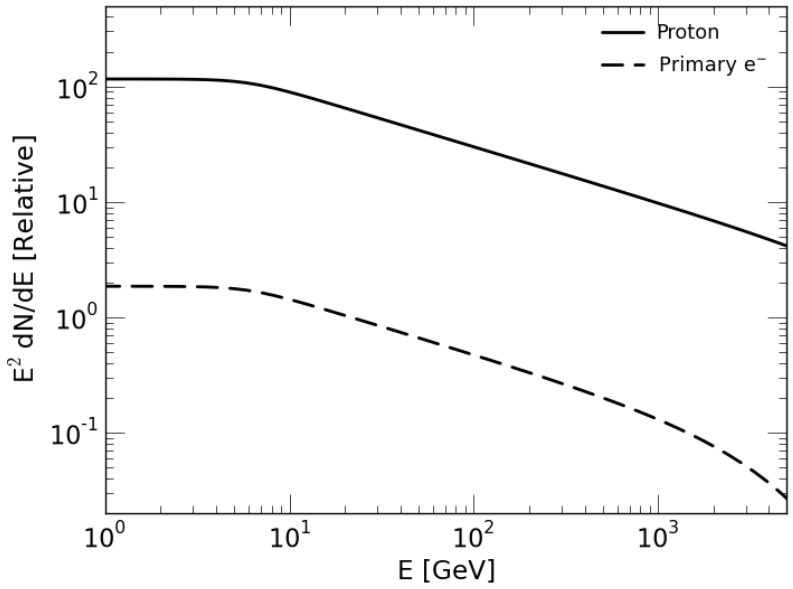

Fig. 2.— The assumed SS injection spectra of protons (solid) and primary electrons (dashed) for the 'SNR-propagation' source class. An exponential cut-off at the maximum energy estimated for an age of 50 kyr is applied to the electron spectrum shown.

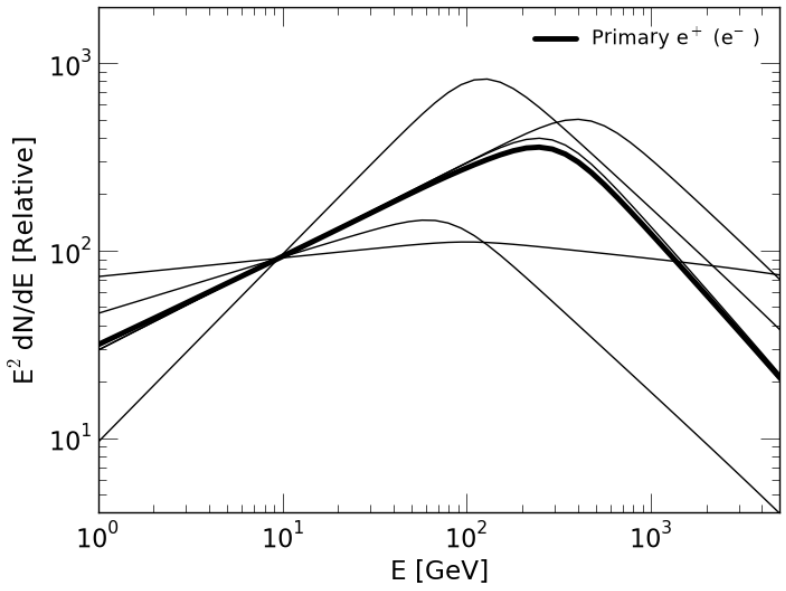

Fig. 3.— Injection spectra of leptons from the 5 PWNe listed in Table 1 (thin lines). The thick solid line is the SS injection spectrum for the 'PWN-propagation' class. All spectra are normalized to each other at 10 GeV for comparison.

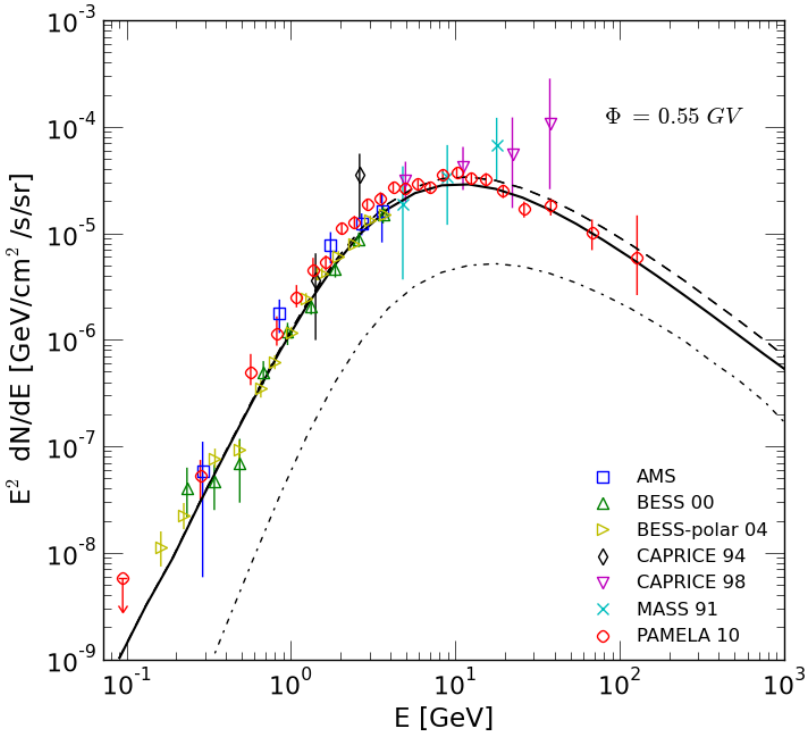

Fig. 4.— Measured CR anti-proton spectra compared with the default model. Anti-protons from the 'SNR-propagation' class are shown by the solid line. For illustration, the contribution from 200 (upper limit) SNR-cloud interaction sites is shown by the dash-dotted line. The dashed line is the sum of the two components.

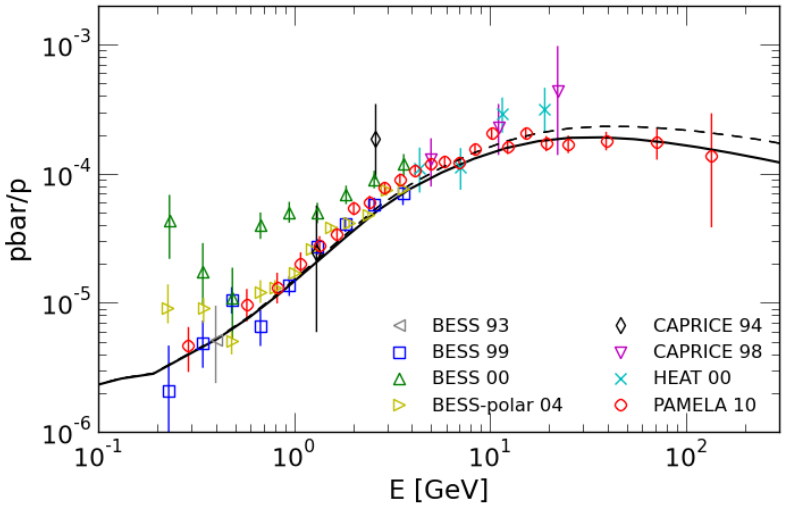

Fig. 5.— Anti-proton-to-proton ratio calculated for the default model compared with measurements. The solid line shows the ratio from the 'SNR-propagation' class only. The dash line shows the ratio including also the contribution of $\bar{p}$ from 200 SNR-cloud interaction sites (dash-dotted line in Fig. 4).

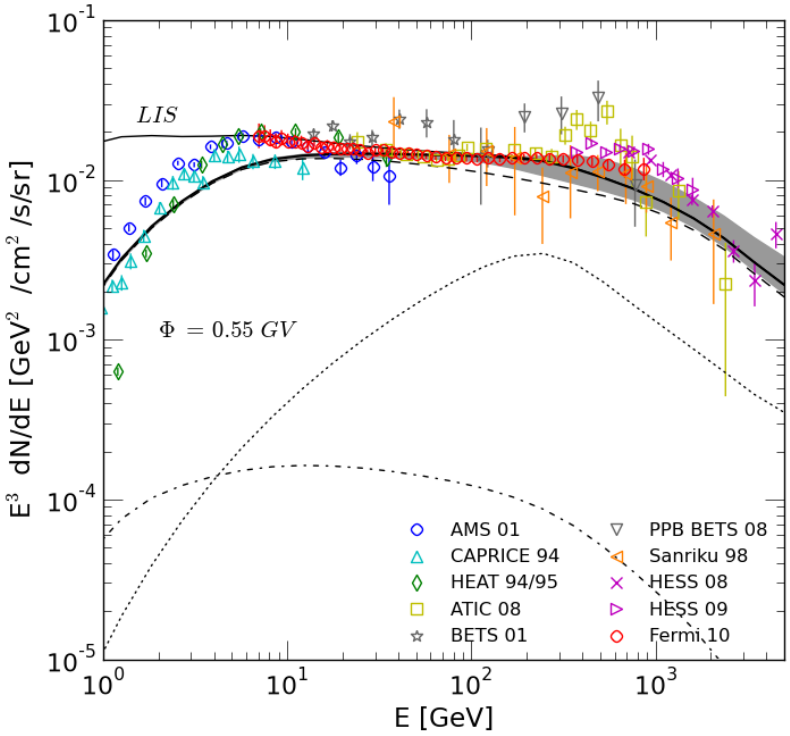

Fig. 6.— Measured CR lepton spectrum compared with the default model (thick solid). The thin solid line shows the local interstellar spectrum (LIS) without solar modulation. Contributions from the 'SNR-propagation' and 'PWN-propagation' source classes are shown by the dashed and dotted lines respectively. The dash-dotted line shows the contribution from 200 SNR-cloud interaction sites. The gray band shows the estimated systematic uncertainty of the total spectrum (see section 5 for description).

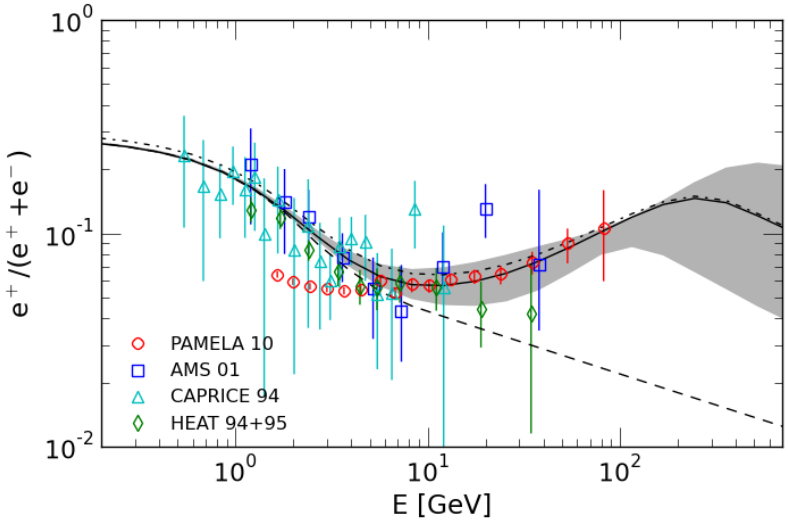

Fig. 7.— Measured positron fraction compared with that calculated using the default model. The fraction calculated for the 'SNR-propagation' class alone is shown by the dashed line. The solid line shows the sum of the 'SNR-propagation' and 'PWN-propagation' components, with the gray band representing the associated systematic uncertainty. The dash-dotted line includes also the contribution from 200 SNR-cloud interaction sites (dash-dotted line in Fig. 6).

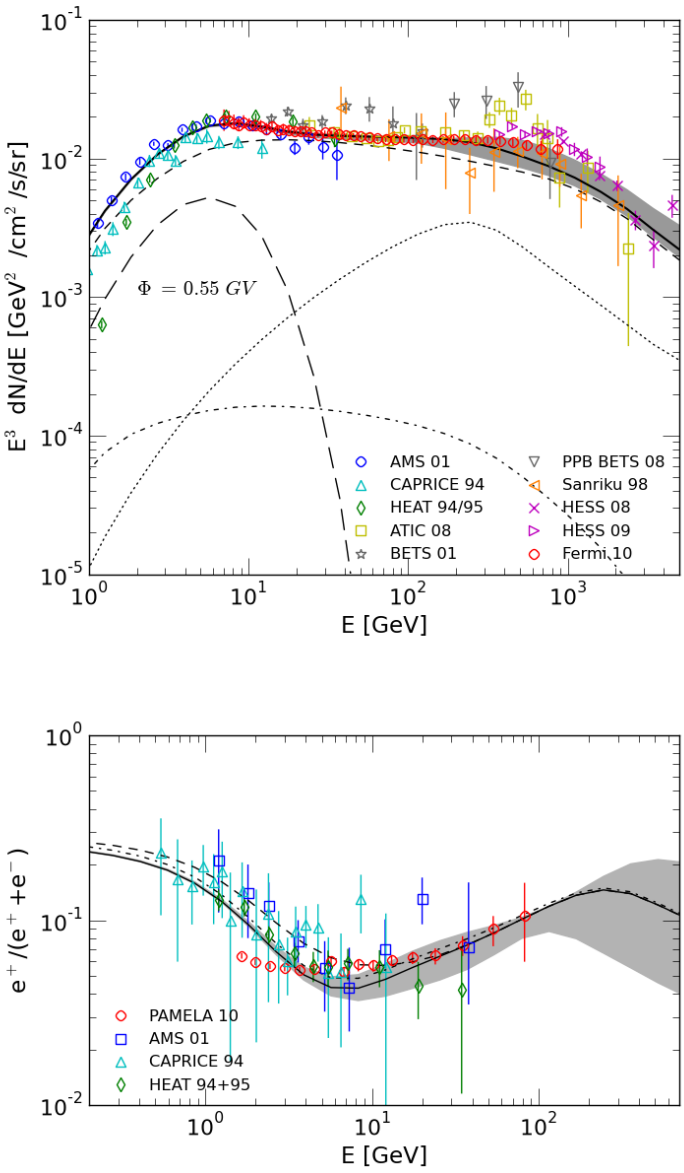

Fig. 8.— Top panel: Measured CR lepton spectrum compared with the default model (thick solid) including a presumed new electron component (long dash). Other lines are identical to those in Fig. 6. Bottom panel: Measured positron fraction compared with that calculated using the default model. The dashed line is the same as the solid line in Fig. 7, while the solid line shows the new fraction taking into account the presumed new electron component. The systematic uncertainty associated with the solid line is again displayed by the gray band. The dash-dotted line shows the positron fraction when contribution from 200 SNR-cloud interaction sites is also accounted for.

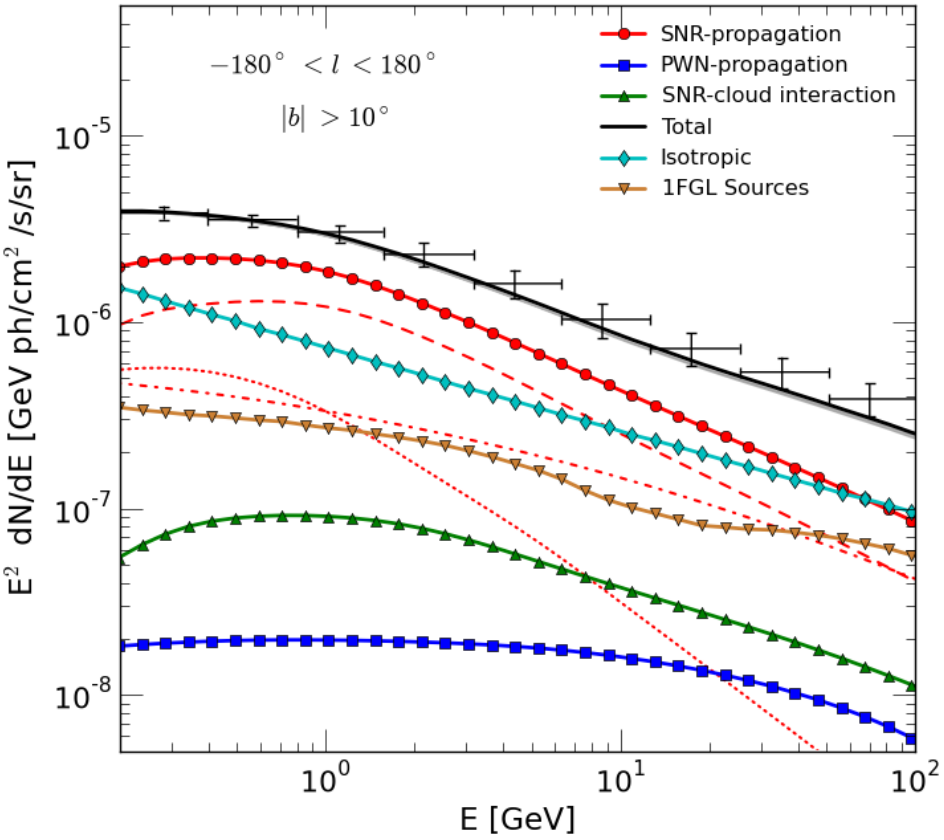

Fig. 9.— Gamma-ray spectrum observed by *Fermi* from the $|b| > 10^\circ$ region (points with error bars) compared with the default model. The total spectrum (solid black) includes the emission produced by SNR-injected CRs (red circles) and PWN-injected CRs (blue squares) during their propagation, the emission from 200 SNR-cloud interaction sites through pion-decay (green triangles), the isotropic background (cyan diamonds), and the sum over the 1FGL *Fermi* catalog point-sources (brown inverted triangles). The emission represented by the red circles consists of pion-decay (red dash), IC (red dot-dash red) and bremsstrahlung (dotted red) contributions. The emission produced by PWN-injected CRs consists predominantly of IC. The *Fermi* data points are taken from Abdo et al. (2010m).